PNAS
www.pnas.org

Supplementary Information for

Two Ck1δ transcripts regulated by m6A methylation code for two antagonistic kinases in the control of the circadian clock.

Jean-Michel Fustin, Rika Kojima, Kakeru Itoh, Hsin-Yi Chang, Ye Shiqi, Bowen Zhuang, Asami Oji, Shingo Gibo, Rajesh Narasimamurthy, David Virshup, Gen Kurosawa, Masao Doi, Ichiro Manabe, Yasushi Ishihama, Masahito Ikawa, Hitoshi Okamura

Jean-Michel Fustin and Hitoshi Okamura
Email: j.m.fustin@pharm.kyoto-u.ac.jp and okamurah@pharm.kyoto-u.ac.jp

This PDF file includes:

Supplementary text
Figs. S1 to S4
Tables S1 to Sx
References for SI reference citations

Other supplementary materials for this manuscript include the following:

Datasets S1 to S2

www.pnas.org/cgi/doi/10.1073/pnas.1721371115

Supplemental Results

CK1δ1 and CK1δ2 lead to different PER2 phosphorylation patterns, insights from mathematical modelling.

In the original model, PER2 phosphorylations by the elusive priming kinase, CK1, and GSK3 (Glycogen Synthase Kinase-3) occurred after translation: PER2 protein first being phosphorylated at S659 or at the β-TrCP site S478, the latter leading to PER2 degradation. When S659 is phosphorylated, downstream sites at S662 and S665 can be sequentially phosphorylated by CK1. Once the FASPS site residues are fully phosphorylated, the CRY (Cryptochrome 1) biding site of PER2 then becomes phosphorylated by CK1 or GSK3, PER2-CRY dimer then entering the nucleus and inhibiting transcription at circadian E-boxes. This sequence of events was modelled to explain the complex 3-step decay dynamics of PER2 proteins. In the original model, it was assumed that the priming kinase, not CK1, phosphorylates S659 but, in our refined model, we instead assumed CK1 does phosphorylate it.

We now ask specifically which PER2 phosphorylation step(s) could be mediated by CK1δ1 and/or CK1δ2 in order to explain their opposite effects on period. Our model showed that when the rate of each phosphorylation step is independently increased by 10%, only that of S659 results in long period, while increasing the rate of all other steps separately, even of the downstream FASPS sites, leads to short period (Fig. S3b). This data predicts that if the rate of S659 phosphorylation is not activated by CK1δ2, no other known CK1 target site on PER2 can explain the period lengthening effects of CK1δ2 overexpression. In addition, inhibiting all steps together, for example in the case of Ck1δ knock-out animals or Ck1δ knock-down cells, would lead to longer period, but inhibiting only the rate of pS659 would cause period shortening (Fig. S3c and d).

Supplemental Methods

Stable transfection of CK1δ expression vectors.

The coding sequence of CKIδ isoforms were cloned into pSELECT-HYGRO-MCS vectors (Invivogen) with the primers 5'-TATGGATCCCAGTAGCGAGCCGCACCGCTGCC-3' and 5'-TATGCTAGCTCATCGGTGCACGACAGACTGAAG-3', respectively containing overhanging BamHI and NheI restriction sites for cloning. Vectors were then transfected into PER2::LUC MEFs with lipofectamine LTX (Invitrogen). 24h after transfection, cells were split into multiple replicate dishes and hygromycin was added to the medium. Medium was changed every three days, with hygromycin, until visible colonies formed. Single colonies were isolated with conventional cloning cylinders then amplified. Monoclonal cell lines were first screened by Western Blot to ensure expression of the appropriate CK1δ isoform.

Other vectors.

5xMyc-mPer2, and the CK1δ1 vector for Fig. 4c were described previously (3, 14). Human CK1δ2 in Fig. 4c was cloned into the same pCS2-MT backbone as hCK1δ1, with 5x myc tag to the N-terminus of its coding sequence, inserted into the plasmid using digestion sites BamH1 and Xba1.

Human PER2 from Fig. 4b, 5b and c was cloned into pSELECT-HYGRO-MCS with the primers 5'-TATGTCGACTCCGAAAGCTTCGTTCCAGAGCCC-3' and 5'-TATGCTAGCTTACGTCTGCTCTTCGATCCTGTG-3', respectively containing the overhang restriction sites SalI and NheI for cloning.
All mutations performed on vectors were carried out by PCR site-directed mutagenesis.

Real-time luminescence measurements.
Cells were seeded into 35 mm dishes or 24-well plates and allow to grow to confluence (typically 3 days). Cells were then shocked by dexamethasone 200 nM for 2 hours, followed by a medium changed including 1 mM luciferine. 35 mm dishes were then transferred to an 8-dishes luminometer-incubator (Kronos Dio, Atto), and 24-well plates to a high-throughput luminometer-incubator (CL24A-LIC, Churitsu). Photons were counted in bins of 2 min (Kronos Dio) or 10 seconds (CL24A-LIC) at a frequency of 20 or 10 min, respectively. Typically, when multiple monoclonal cell lines were to be simultaneously analyzed (Fig. 3e), the CL24A-LIC was used.

Culture of adult primary skin fibroblasts
6-weeks old -43/-43 and wild-type mice were sacrificed by cervical dislocation and fully dipped into 70% ethanol for 5 minutes with agitation. Ears and skin from the entire tail were excised, transferred to a new Petri dish and brought in a clean bench. Ears and tail skin were transferred twice to a new Petri dish containing 20 ml Hank's Balanced Salt Solution (HBSS) with calcium and magnesium. In the second HBSS wash, tissues were finely chopped with blunt scissors, pieces were transferred to a new dish with 10 ml HBSS containing 1 U/µl type II Collagenase (Gibco), and digested for 8 hours at 37°C, 5% CO_2. Cells and tissues were mixed by pipetting several times and collected into a 15 ml tube and centrifuged at 400xg for 5 min. Tissues were resuspended in fresh warm 10 ml HBSS containing 1 U/µl type II Collagenase and transferred to new Petri dishes and incubated at 37°C, 5% CO_2 for another 2 hours. 5 ml of F12/DMEM containing L-Gln, sodium pyruvate and HEPES with 10% FBS and penicillin/streptomycin/amphotericin A was added to each dish and incubation was pursued overnight. The next day tissues were collected by pipetting to 15 ml tubes, centrifuged at 400xg for 5 min, washed once then centrifuged and resuspended again in 10 ml of the F12/DMEM described above, then transferred to new Petri dishes. After 2-3 days or growth medium was removed along with floating tissues and hairs, cells were trypsinized and passaged using conventional methods. All experiments described with these cells were completed before 6 passages.

siRNA mediated gene silencing
Silencing was performed with Stealth siRNA from Invitrogen. Sequences and IDs are given in supplemental methods. MEFs plated in 24-well plates at 70,000 cells/ml were transfected the next day with 40-80 pmol siRNA using 3 µl/well Lipofectamine 3000 (Invitrogen). For protein analysis by Western Blot shown on Fig. 1b, cells were sampled 48h later. For PER2::LUC cells and real-time luminescence shown in Fig. 5a, cells were plated at 70,000 cells/ml in 35 mm dishes, transfected the next day with 320 pmol siRNA and 16 µl Lipofectamine 3000. Sixteen hours later, medium was changed (antibiotics omitted), and 8 hours later cells were synchronized by a dexamethasone shock as described above. For the FASPS data on Fig. 5b, human U-2 OS cells plated at 150,000

cells/ml were plated in 24-well plates and transfected the next day with 70 pmol siRNA and 3.5 µl lipofectamine 3000. Sixteen hours later medium was changed (minus antibiotics), 8 hours later cells were synchronized by a dexamethasone shock as described above. Cells were lysed in 2x SDS sample buffer the next day, 28h after dexamethasone shock, which correspond to time of high PER2 expression.

Co-immunoprecipitation for immunoblot

HA-tagged or MYC-tagged CK1δ1 were co-transfected with MYC-tagged or HA-tagged CK1δ2, respectively, together with 5xMYC-PER2. Cells were lysed on ice in 50 mM Tris, 600 mM NaCl,1% NP40, 0.5 mM DTT, 10% glycerol with complete protease inhibitor +EDTA (Roche) and Phostop (Roche). Cell lysates were diluted 5 times in 50 mM Tris, 0.5 mM DTT, 10% glycerol with complete protease inhibitor +EDTA (Roche) and Phostop (Roche), and immunoprecipitated using agarose-protein G beads (Roche) coupled to αHA antibody (Roche 11867423001) using standard procedures.

Immunoblot

Direct cell lysis using 2x Laemmli buffer supplemented with complete protease inhibitor +EDTA (Roche) and Phostop (Roche) followed by 10 min boiling at 95°C was used in all experiments. Immunoblots were performed following standard procedures for migration and blotting with mini-gel (ATTO, Japan). For Fig. 3f, pre-cast Phos-tag (WAKO, Japan) 6% acrylamide gels were used. Experimental details for each antibody used were: for CK1δ, Proteintech 14388-1-AP, 750x; for Mettl3, Proteintech 15073-1-AP, 750x; for Mettl14, Atlas HPA038002, 250x; for Actin, Sigma A5441, 1000x; for Myc, Sigma C3956, 2000x; for hFASPS, Millipore ABN299, 250x; for RPLP0, Proteintech 11290-2-AP. The rabbit polyclonal antibody against phospho-Ser 659 of mouse PER2 was developed at Abfrontier (Young In Frontier Co.) using the phospho-peptides GKAEpSVVSLT-Cys (Narasimamurthy, this issue of PNAS). The rabbit affinity-purified anti-PER2 was previously described (15).

Liver mRNA preparation and me-RIP

Total RNA was extracted from liver samples using Qiagen RNeasy midi kit. mRNA was then purified from total RNA using NEBNext Poly(A) mRNA Magnetic Isolation Module (NEB), followed by an additional purification step using Qiagen RNeasy MinElute columns. The mRNA was further fragmented using NEBNext Magnesium RNA Fragmentation Module (NEB), also followed by an additional purification step using Qiagen RNeasy MinElute columns. Methylated fragmented mRNA was then immunoprecipitated using protein A agarose beads (Roche) coupled to anti-m6A antibody (202003, SYSY). 50ul beads were incubated with 10ug antibody in 0.1 M PBS, T-X100 0.01%, 0.1mg/ml BSA (IP buffer) for 2h at 4°C in a rotator. Beads-Ab were then washed 3 times with 1 ml IP buffer, then resuspended in 1 ml IP buffer with 5 µg 40-mer polyA, and incubated 1h at 4°C for pre-blocking. Beads-Ab were washed once with 1ml IP buffer, then resuspended in 400 µl IP buffer. 5 µl RNasin PLUS (Promega) were added to the beads-Ab, followed by 2 µg fragmented mRNA; the mix was incubated 2h at 4°C in a rotator. Beads were then washed 3 times with 0.4 ml IP buffer with RNasin PLUS at 4°C, then 2 times at RT. The final beads pellet was resuspended in 700 µl RLT buffer from Qiagen MinElute kit, vortexed at full speed 10 sec 5 times and centrifuged at

1000xg. The supernatant containing extracted methylated fragmented mRNA was transferred to a new tube and processed according to Qiagen MinElute protocol. cDNA library was synthesized as described previously (16).
For qPCR quantification of m6A, a similar procedure was used but unfragmented mRNA was directly immunoprecipitated using 8 μg of anti-m6A antibody per 500 ng mRNA for 100 μl bead slurry. IP was performed at 4°C in 200 μl of the same IP buffer as above using a thermomixer (Eppendorf) at 1000 RPM 30 sec off 30 sec on. After IP the supernatant (200 μl) was mixed with 700 ul RLT buffer (Qiagen) with mercaptoethanol and vortexed 10 sec at full speed. After washing, beads were mixed with IP buffer to a volume of 100 μl then mixed with 350 μl RLT buffer with mercaptoethanol. mRNA from supernatant and beads was purified using Qiagen MinElute protocol, from which the whole eluate was reverse transcribed (VILO cDNA synthesis kit, Invitrogen). Absolute copy numbers of target cDNA in the input and supernatant samples were quantified with SYBR Green PCR Master Mix (Invitrogen). Tbp, a weakly or unmethylated transcript (no significant peak), was used as a normalizer.

Me-RIP RNA-seq and Tuxedo protocol.
Reads from input and Me-RIP Fastq files were first trimmed (Trimmomatic) and aligned to the reference genome mm10 with Tophat (17) setting the –segment-length option to 18 and –read-realign-edit-dist to 0. Peak Calling was performed for each time point by MACS2 (18) using sorted bam files. IntersectBed was used to determine peaks detected in 1 or 2 time points. To visualize peaks, MACS2 bdgcmp was performed on the treatment (me-RIP)- and control (input)-bedgraph outputs from MACS2 to deduct noise from me-RIP samples. These analyses were performed on the Galaxy server.

Polyribosome fractionation
24 hours before sampling, sucrose gradient was built by successively underlaying 2.2 ml of 10%, 20%, 30%, 40% and 50% sucrose solutions (Tris-HCl pH 7.5 20mM, MgCl2 10mM and KCl 100mM, 2mM DTT, murine RNase Inhibitor NEB 5ul/1000ul and cycloheximide 100 μg/ml) in 12 ml ultracentrifuge tubes (Beckman, 344059) using a Pasteur pipette mounted on a SOCOREX macropipette. Gradients were left for at least 24h at 4°C. The next day, ~80% confluent cells in 15 cm dishes were washed twice with ice-cold PBS, then incubated for 5 min in ice-cold PBS containing 100 μg/ml cycloheximide. PBS was decanted and cells were harvested on ice and transferred to a cold 2 ml microtube.
Cells were centrifuged at 500xg for 5 minutes at 4°C. Supernatant PBS was discarded and cells were lysed in 6x of cell weight lysis buffer (20 mM Tris-HCl pH 7.5, 10 mM MgCl2, 100 mM KCl, 1% NP40, supplemented with EDTA-free cOmplete Protease Inhibitors (Roche), 2mM DTT, murine RNase Inhibitor (NEB, 1μl/40ul) and cycloheximide (100 μg/ml) for 10 min on ice after being passed 5 times through a 25G needle. The lysates were centrifuged 1300xg for 10 min at 4°C and the cleared lysates were transferred into new cold 1.5 ml tubes and kept on ice. 250 μl of cleared cell lysate was then carefully added on top of the sucrose gradient, one gradient for each lysate sample, and gradient were centrifuged at 36,000 RPM (Beckman Optima L ultracentrifuge, SW41 Ti rotor) at 4°C for 2 hours, with lowest acceleration and no brake. After centrifugation, each gradient was then split into 21 fractions by collecting 500 μl

aliquots from the top of the gradient, all steps performed at 4°C. Each fraction was mixed with 1500 µl Trizol LS (Invitrogen). RNA from each fraction was extracted following manufacturer's protocol and resuspended in the same volume of RNAse-free water (50ul/fraction). Same volumes of RNA were then used for cDNA synthesis (VILO cDNA synthesis kit, Invitrogen). Transcript abundance in each fraction was quantified by quantitative real-time PCR with SYBR Green PCR Master Mix (Invitrogen), using the deltaCT method. The first (top most in the gradient) fraction was discarded from the data, as it contained no detectable mRNA, and the next fraction from the top of the gradient was used as a reference and set to 1 in each gradient data series.

Protein alignment and structure predictions
Amino acid sequences were aligned by PRALINE to obtain color-coded amino acid conservation (http://www.ibi.vu.nl/programs/pralinewww/) (19).

CRISPR-Cas9 genetic editing
EGR-G101 ES cells (C57BL/6 background) were transfected with the pX330 (20) plasmid carrying gRNA sequence, 5'-AAAACACAAACTAAATGGAC-3'. After clonal expansion, the target region was amplified by PCR with primers (5'-GGGTGTGCCTGTTCTCTCTAGG-3' and 5'-TACACAACTGATGAGAAGTTCC-3') and subjected to Sanger sequencing. A clone carrying the -43/-43 mutation was then injected into ICR 8-cell embryos to generate chimeric male mice, and the germline transmission of the mutant allele was confirmed by PCR after mating with wild-type C57BL/6 female mice. Genotyping was carried out by conventional PCR using the primers 5'-GCACCGATGAGAACTCTCCT-3' and 5'-GTCTCCCAGCCTCTGCTCTT-3'.

Primer and siRNA sequences
Quantitative real-time primer sequences were: for *Ck1δ2* 5'-CTGCTCGTCTCCATCGGAAG-3' and 5'-TTGGTAACAGAGTAGATCAGCC-3', for Ck1δ1 5'-CATGTCCACCTCACAGATTCC-3' and 5'-TTGGTAACAGAGTAGATCAGCC-3, for *Ck1ε* 5'-GAGACATCTACCTGGGTGCCA-3' and 5'-ACCACTTGATGGACGGGATC-3', for *Rplp0* 5'-CTCACTGAGATTCGGGATATG-3' and 5'-CTCCCACCTTGTCTCCAGTC-3', for *Mettl3*, 5'-TGATCTGGAGATAGAAAGCC-3' and 5'-CAACAATGGACTGTTCCTTG-3'.
RNAi was performed with Stealth siRNA from Invitrogen: custom 5'-GGGATATTCACATGGAGCTACCGTA-3' for *Mettl3*; custom 5'-GCATTCCTTTCGAACACCACGGCAA-3' for *Ck1δ2*; for *Per2*, PER2MSS207536, (MSS207537, MSS207538 gave similar results); for pan*Ck1δ*, CSNK1DHSS102382, (CSNK1DHSS102383, CSNK1DHSS175379 worked equally).

In vitro transcription and translation
The 5'-UTR of Csnk1d was cloned into a pGL4.12 backbone (Promega) upstream of the destabilized luciferase LUC2CP coding sequence, and the 3'-end of the *Ck1δ1* or *Ck1δ2* coding sequences, followed by their respective 3'-UTRs, were cloned downstream of the LUC2CP STOP codon. A 1838 bp deletion of the 3'-UTR was achieved by conventional

sequential PCR rounds to truncate the 3'-UTR region between the native NsiI and MfeI restriction sites. Essentially, the 5'-GATCTACTCTGTTACCAATG-3' upstream sequence in the 3'-UTR was joined to the 5'-ACTAGGACCATTGGAAGTCC-3' downstream. Linear templates for in vitro transcription were then amplified by PCR, with the 5'-TAATACGACTCACTATAGGGAGAAGTGACGTCACAGCGCGATGGCGG-3' forward and 5'-GAGGGAAGAAAGGTAGAAGTCATTATG-3' reverse primers. The forward primer contained a T7 promoter overhang (underlined) for in vitro transcription. Messenger RNAs were transcribed in vitro using the mMESSENGER mMACHINE T7 ULTRA kit (Invitrogen) following manufacturer's protocol. A control mRNA containing the Renilla luciferase coding sequence was also in vitro transcribed from the pRL-SV40 linearized vector (Promega). To confirm specificity of transcription, after purification all mRNAs were checked by denaturing agarose gel electrophoresis and quantified.
For in vitro translation, the Flexi Rabbit Reticulocyte Lysate System (Promega) was used following manufacturer's instructions. For each condition, equal number of copies of the appropriate Ck1δluc transcript were added to the lysate together with Renilla control mRNA. After 2h incubation, reaction was stopped with passive lysis buffer (Promega) and endpoint luminescence was measured by Dual Luciferase Assay (Promega).

Mathematical modelling

In the original model, the circadian protein complex was represented as x[j][k][l][m][n] due to the large number of variables, where j, k, l, and n correspond to the status of proteins, PER, CRY, Kinases (Priming kinase, CK1 and GSK3) and BMALs-CLOCK, respectively, and m corresponds to the subcellular location of the complex.
The modified code used was:

```
x[j][k][l][m][n](t)'=
If[((j==3))&&((l==1)||(l==3))&&(k==0),-bto*x[j][k][l][m][n](t),0]+
If[((j==10))&&((l==1)||(l==3))&&(k==0),bto*x[3][k][l][m][n](t),0]+
If[((j==7))&&((l==1)||(l==3))&&(k==0),-hto7*x[j][k][l][m][n](t),0]+
If[((j==8))&&((l==1)||(l==3))&&(k==0),hto7*x[7][k][l][m][n](t),0]+
If[((j==8))&&((l==1)||(l==3))&&(k==0),-hto8*x[j][k][l][m][n](t),0]+
If[((j==9))&&((l==1)||(l==3))&&(k==0),hto8*x[8][k][l][m][n](t),0]+
If[((j==9))&&((l==1)||(l==3))&&(k==0),-hto9*x[j][k][l][m][n](t),0]+
If[((j==4))&&((l==1)||(l==3))&&(k==0),hto9*x[9][k][l][m][n](t),0]+
If[((j==5))&&((l==1)||(l==3))&&(k==0),-hto5*x[j][k][l][m][n](t),0]+
If[((j==6))&&((l==1)||(l==3))&&(k==0),hto5*x[j-1][k][l][m][n](t),0]
```

, in which hto5, hto7, hto8, and hto9 are expressed by a single parameter hto in the original model.
Period sensitivity was first analyzed using this model with original parameters. For period sensitivity with respect to multiple parameters (Fig. S3c), bto, hto5, hto7, hto8, hto9, and pto were increased simultaneously by multiplying by the same factor. To examine the generality of the results for period elasticity, we then repeated the same analysis for 100 randomly generated parameter sets, each rate parameter kept uniformly distributed between double or half the original value, except for Nf, the nucleus-cytosol ratio. Period elasticity with respect to each phosphorylation process r_i, defined as: $\delta \ln \tau / \delta \ln r_i$ (21). The code used in this paper is available on request.

Co-immunoprecipitation for LC-MS/MS analysis

Cells transfected in five replicate 20 cm dishes for each transfection mix were washed with ice-cold PBS, harvested and pooled in PBS, and cell pellet was lysed with lysis buffer (50 mM HEPES (pH 7.5), 140 mM NaCl, 1 mM EDTA, 10% glycerol, 0.5% NP-40, 0.25% Triton X-100, protease/phosphatase inhibitor cocktails). The lysates were clarified by centrifugation at 12,000 x g for 20 minutes at 4°C and the protein concentration was determined by BCA assay. 5 mg of protein lysate was precleared with isotype control IgG and magnetic Dynabeads Protein G before incubating with 50 μg anti-Myc antibody (Sigma C3956 lot 094M4755V and 016M4762V) at 4°C overnight followed by 2-hour Dynabeads Protein G incubation. After washing the beads with lysis buffer 4 times, TBS 2 times and deionized water 2 times, the immunoprecipitates were eluted with urea buffer (8 M urea, 10 mM Tris-HCl, pH 8.0).

Sample preparation and nanoLC-MS/MS analysis

The eluent was reduced with 10 mM DTT, alkylated with 50 mM IAA, and digested with Lys-C at 37°C for 3 hours. Samples were 5-fold diluted with 50 mM ammonium bicarbonate followed by trypsin digestion at 37°C overnight. The digest was desalted and clarified with SDB-XC-SCX StageTips (22). After desalting, peptides were measured by Q-Exactive mass spectrometer (Thermo Fisher Scientific), connected to a Thermo Ultimate 3000 RSLCnano pump and a HTC-PAL autosampler (CTC Analytics) equipped with a self-pulled analytical column (150 mm length × 100 um i.d.) packed with ReproSil-Pur C18-AQ materials (3 μm, Dr. Maisch GMBH). Peptides were separated by 5–10% B in 5 min, 10–40% B in 60 min, 40–100% B in 5 min, 100% B for 10 min, and 5% B for 30 min (Solvent A was 0.5% acetic acid and solvent B was 0.5% acetic acid in 80% acetonitrile) at a flow rate of 500 nl/min. The applied voltage for ionization was 2.4 kV. The MS scan range was m/z 350–1500 at a resolution of 70.000 (at m/z 200) in the orbitrap using an AGC target value of 3 × 106. The top ten precursor ions were selected for subsequent MS/MS scans in the HCD (higher-energy collision) cell and acquired at resolution 17.500 (at m/z 200) in the orbitrap using an AGC target value of 1 × 105. Dynamic exclusion was applied for 30 sec. Peptides were identified as described in the Supplemental methods.

Peptides identification after nanoLC-MS/MS

Peptides and proteins were identified by means of an automated database search using Mascot version 2.5.1 (Matrix Science) against SwissProt Database (version 2015_02) with a precursor mass tolerance of 5 ppm, fragment ion mass tolerance of 0.02 Da, and strict trypsin specificity allowing for up to two missed cleavages. Cysteine carbamidomethylation was set as a fixed modification, and methionine oxidation and the phosphorylation on serine, threonine, and tyrosine were allowed as variable modifications. Peptides were considered to be identical if the Mascot score was over the 95% confidence limit based on the identity score of each peptide. False discovery rates (FDRs) were estimated by searching against a randomized decoy database (<1%). Phosphorylation site localization was confirmed based on the presence of site-determining ions and the Mascot Delta Score (≥10). No peptides detected in bead controls were included. The results of label free quantitation were confirmed by manual inspection for extracted ion current of each peptide. For protein quantification, the total

peak area of the peptides was used. To determine the phosphorylation levels of each identified phosphosite on PER2, the peak area was normalized to the level of PER2 in each sample.

Serine, threonine and tyrosine sites were classified into three groups: (1) phosphorylated sites unambiguously identified based on phospho-site determining product ions, (2) unphosphorylated sites based on nonphospho-site determining ions, and (3) possibly phosphorylated sites speculated by only precursor ions without site determining ions. Each serine, threonine, and tyrosine on identified PER2 phosphopeptides was annotated using a color code in Fig. S4a, and typical MS/MS spectra of identified phosphorylated FASPS are shown in Fig S4b, with the 3-phopshorylated FASPS peptides (m/z = 898.6989 ± 10 ppm) containing product ions for determining phosphosite localization corresponding to the four isoforms listed in Fig. S4a. The tryptic phosphopeptide ranging from residue 557 to 679 of PER2 was repeatedly identified in CK1δs overexpressing samples with product ions, and some of which are site determining ions for specific phosphosites and unphosphorylated sites. For instance, phosphorylation on S662 in the first spectrum (Fig S4b1) was determined by the coexistence of b7 and b3 or b4 ions. The b7 ions indicated one phosphorylation was observed between A557 and L662 which contains two possibly phosphorylated serine residues. In parallel, the b3 or b4 ions excluded the possibility of phosphorylation on S659, confirming S662 is the only possible phosphorylation site between 557 and 662. The same rule was applied for other phosphopeptide isoforms (Fig. S4b2-6). However, we still couldn't exclude the possibility that spectrum S4b1, S4b2 and S4b3 were derived from the same form of 3-phopshopeptide. From the data, we can identify at least two types of phosphorylated isoforms, pS659- or pS662- containing peptides, which were co-eluted at similar retention time. As for the 2- and 4- phosphopeptides, only one phosphopeptide isoform was identified based on site determining product ions, suggesting at least one type of 2- and 4- phosphopeptides isoform were present (Fig S4a).

Supplemental Discussion

Although the observation presented on the activity of CK1D isoforms need to be confirmed in in vitro kinase assays, our data show that CK1δ2 may be the priming kinase that allows the phosphorylation of downstream residues in the FASPS cluster. When CK1δ2 increases, alone or together with CK1δ1, the phosphorylation of the FASPS cluster increases and the period elongates. When the presence of two isoforms is ignored, this statement may seem contradictory to reports showing long period in Ck1δ knock-out cells (1, 2). Similarly to what has been proposed by the phosphoswitch model (3), however, the phosphorylation by CK1δ2 may protect PER2 from being phosphorylated at the β-TrCP site by CK1δ1, making the FASPS site the only available target for CK1δs-mediated phosphorylation, increasing the period. When the Ck1δ gene is knocked-out or when both isoforms are knocked-down, the lack of β-TrCP site phosphorylation will also lead to lower degradation rates of PER2 and to long period.

In the case of an increase in total CK1D activity, we propose the ratio is important. For a low CK1δ2/1 ratio such as in the brain, an increase in CK1δ activity from zero may initially shorten the period until β-TrCP site phosphorylation reaches near maximal rate, beyond which further CK1δ increase would lead to period elongation due to enhanced FASPS site phosphorylation. For a mid-to-high CK1δ2/1 ratio, CK1δ2-mediated FASPS site phosphorylation would protect PER2 from β-TrCP site phosphorylation, and an increase in total CK1δ in this case would elongate the period.

In the case of a change in ratio, such as in CK1δ1 or CK1δ2 overexpression from a vector or isoform-specific knock-down, increase or decrease in CK1δ2/1 will respectively lead to long or short period as the competition between isoforms progresses. That CK1δ2 may stabilize PER2 only in the presence of CK1δ1 may also explain why transfected PER2 was not stabilized with CK1δ2 in Fig. 5c. Whether circadian period control via dynamic changes in CK1δ balance occurs in vivo, for example as a mechanism underlying temperature compensation to slow or accelerate the clock in response to temperature changes, and whether CK1δ isoforms expression is matched to the amount of PER2 and other targets, remain to be investigated. And when CK1ε is put into the picture, more questions arise about the interactions and specific functions of CK1 kinases. Isoform-specific knock-out mice, as well as CK1δ1 or CK1δ2 Rosa26 knock-in mice will be instrumental to resolve these questions.

The β-TRCP site was not investigated here since it was not detected in our LC-MS/MS analysis, but the activity of CK1δ1 and CK1δ2 on this site may also be different, and the differences between CK1δ1 and CK1δ2 may go well beyond the phosphorylation of PER2. Structure predictions revealed that, while the CK1δ1 tail IPGRVASSGLQSVVHR assumes a coiled-sheet conformation, the shorter NSIPFEHHGK tail of CK1δ2 instead forms a helix. In addition, S406, S407 and S411 in the CK1δ1 tail are potentially isoform-specific regulatory phosphorylation sites (4, 5), probably underlying the inhibitory effect of the CK1δ1 tail on priming kinase activity (Narasimamurthy, this issue of PNAS). Interestingly, the C-terminal tail of CK1ε is more similar to that of CK1δ2, CK1ε indeed having high priming kinase activity (Narasimamurthy, this issue of PNAS). The ability of full-length CK1ε to apparently fully phosphorylate PER2 has been previously suggested (6).

As has been demonstrated for the entire AGC kinase family, the C-tail wraps around the two lobes of the kinase core and is essential for its activity and is a hallmark for functional divergence (7). The last ~10 amino acids of the C-tail, named the N-lobe tether, is a docking site for interactions with other proteins. We propose a similar role for the C-tail of CK1δ isoforms. Unfortunately, due to the difficulty in crystallizing full-length CK1δ or ε, the structure and function of the C-domain remains unknown to this date.

Interestingly, we have noticed that the expression of CK1δs changes in correlation with the confluency of the cell population in PER2::LUC MEFs, and may be related to m6A levels. For example, compare Fig. 1a, showing data from a 100% confluent cell

population, with Fig. 1b, showing data from a ~60% confluent population (as required for siRNA transfection). Since CK1δ has been involved in the regulation of the cell cycle, it is likely that the two isoforms will also have different functions in this process, maybe in the phosphorylation of WEE1 (8).

The methylation in the *Ck1δ* 3'-UTR, and the increase in translation when it is inhibited, as well as the short half-life especially for *Ck1δ1*, together indicate that *Ck1δ* mRNAs are dynamically regulated transcripts that must respond quickly to a change in conditions. The involvement of CK1δ in the cell cycle, where its expression rises during S to G2 phases (8), is in line with this. To our knowledge, however, no clear circadian rhythms of steady-state *Ck1δ* mRNA or protein levels have been reported. It would be interesting to investigate what is the stability of a single kinase in vivo, as CK1δ may work like a "kamikaze" kinase, and immediately degraded upon phosphorylating a substrate. The fact that CK1δ can inactivate itself by auto-phosphorylation (9) indeed suggests that its activity is ephemeral, and in line with a tightly-regulated mRNA.

One outstanding question, pervasive in m6A research, is whether and how m6A can be dynamically regulated in adult animals (10, 11). The expression of CK1δ isoforms, as well as other m6A-methylated transcripts, might be dynamically regulated by m6A in response to physiological or pathological conditions. Why *Ck1δ* mRNAs have such different half-lives, and how the splicing choice between the two isoforms is regulated in different tissues, have not been investigated here. Different secondary structures of *Ck1δ* transcripts, together with m6A methylation, may provide substrate for tissue-specific RNA-binding proteins regulating the balance between CK1δ isoforms via splicing and/or mRNA stability regulation. In a circadian context, the tissue-specific CK1δ2/CK1δ1 ratio may explain variations in clock period observed from different tissues measured in vitro (12).

These data are reminiscent of a recently identified shorter isoform of DOUBLETIME (DBT), the homologue of CK1δ/ε in Drosophila (13). This new isoform, translated from an alternative initiation site, is shorter and believed to have no kinase activity. When expressed together with the full length DBT, however, this short isoform caused period elongation in locomotor activity rhythms by delaying PERIOD protein degradation. As far as we know from available information, CK1δ1 and CK1δ2 are conserved in all vertebrates (Fig. S1d), but antagonistic CK1δ isoforms may well be found in other organisms.

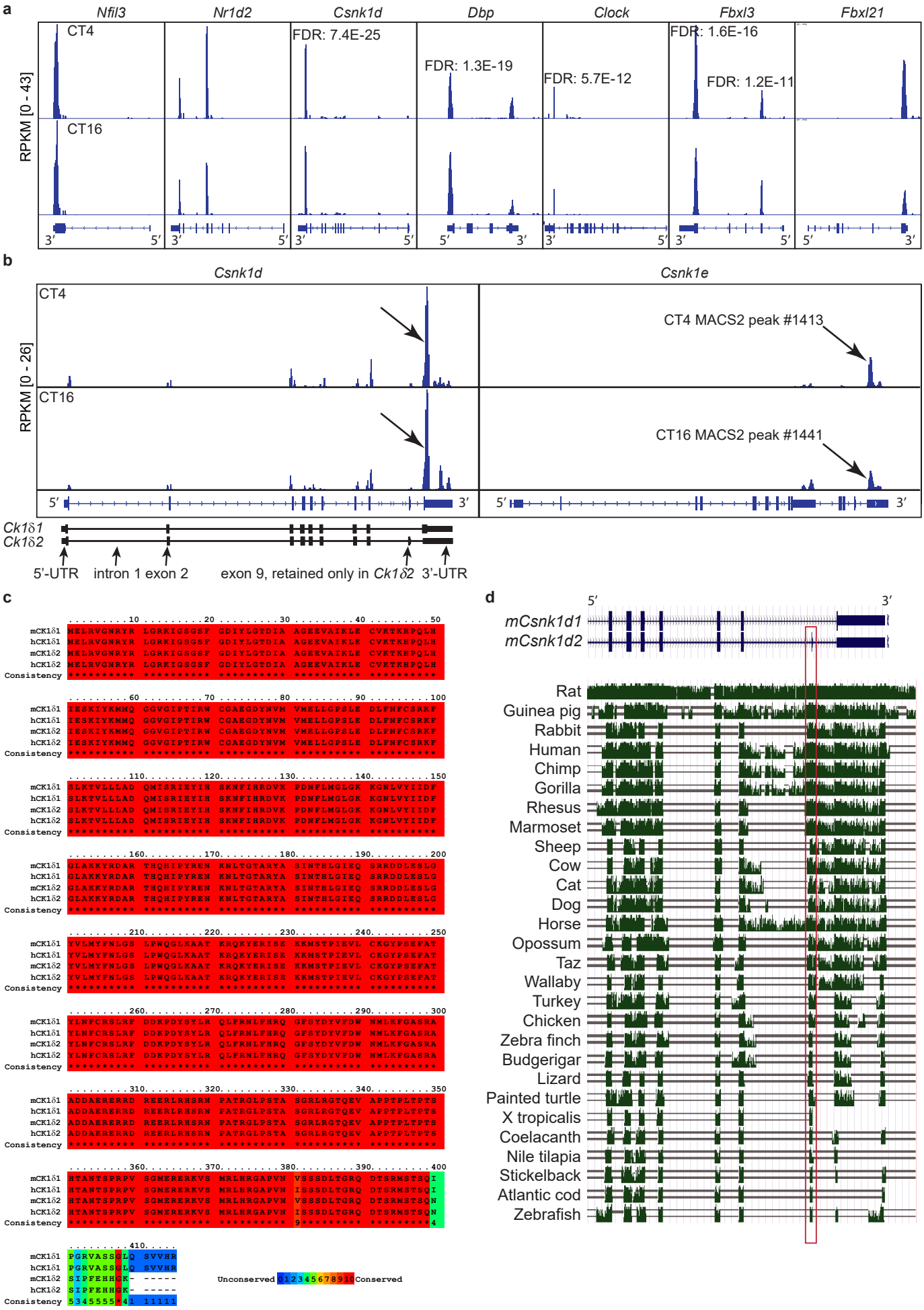
a
Nfil3
Nr1d2
Csnk1d
Dbp
Clock
Fbxl3
Fbxl21
CT4
CT16
RPKM [0 - 43]
FDR: 7.4E-25
FDR: 1.3E-19
FDR: 5.7E-12
FDR: 1.6E-16
FDR: 1.2E-11
3′
5′
b
Csnk1d
Csnk1e
CT4
CT16
RPKM [0 - 26]
CT4 MACS2 peak #1413
CT16 MACS2 peak #1441
Ck1δ1
Ck1δ2
5'-UTR
intron 1 exon 2
exon 9, retained only in Ck1δ2
3'-UTR
c
mCK1δ1
hCK1δ1
mCK1δ2
hCK1δ2
Consistency
Unconserved 0 1 2 3 4 5 6 7 8 9 10 Conserved
d
mCsnk1d1
mCsnk1d2
Rat
Guinea pig
Rabbit
Human
Chimp
Gorilla
Rhesus
Marmoset
Sheep
Cow
Cat
Dog
Horse
Opossum
Taz
Wallaby
Turkey
Chicken
Zebra finch
Budgerigar
Lizard
Painted turtle
X tropicalis
Coelacanth
Nile tilapia
Stickelback
Atlantic cod
Zebrafish

Fig. S1. Two highly methylated alternative Ck1δ transcripts are conserved in vertebrates and code for two CK1δ isoforms with different C-terminal tails.

(**a**) Integrative Genomic Viewer visualization of me-RIP RNA-seq data of clock-related transcripts with significant m6A levels. Upper panel, data at CT4; middle panel, data at CT16; lower panel, transcript organization, with introns shown as thin blue lines and exon as thick blue segments. The False Discovery Rate (FDR) is given at the top of each significant peak for *Ck1δ*, *Dbp*, *Clock* and *Fbxl3*. *Csnk1d* is the gene name for *Ck1δ*. (**b**) Integrative Genomic Viewer visualization of me-RIP RNA-seq data of *Ck1δ* and *Ck1ε* transcripts at CT4 and CT16, with the transcript organization at the bottom. As indicated by black arrows, compare the height of the significant *Ck1δ* peak in the 3'-UTR, compared to the non-significant one in *Ck1ε*' s. At the bottom of the Ck1δ panel is shown the organization of the two alternative transcripts of *Ck1δ* (**c**) CK1δ1 and CK1δ2 amino acid sequences of human and mouse aligned with PRALINE. (d) UCSC Genome Browser view of the 3' end of the Csnk1d gene in vertebrates. The area indicated in red correspond to the exon 9 of *Ck1δ2* ; note the conservation of this exon among all vertebrate species. The blue schema on top shows transcript structures, the green plot underneath indicates sequence conservation.

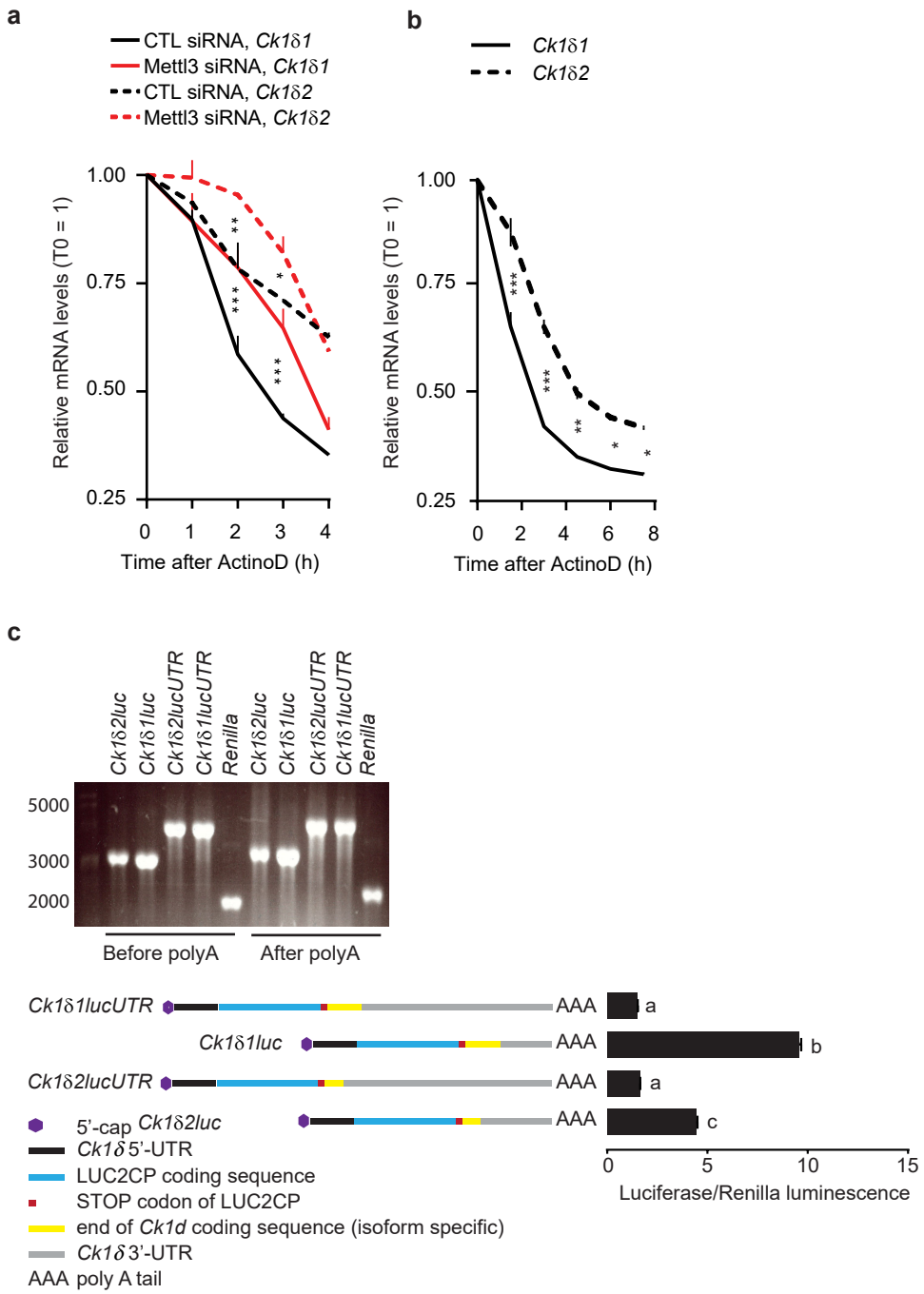

Fig. S2: Post-transcriptional regulation of *Ck1δ1* and *Ck1δ2* mRNAs.

(**a**) Mettl3 silencing caused a significant delay in the initial steps of *Ck1δ* mRNA turnover, analysed by Two-Way ANOVA followed by Bonferroni post-test, shown mean +/- SEM, n=3, *=p<0.05, **=p<0.01, ***=p<0.001. Note the different half-life for *Ck1δ1* and *Ck1δ2*, confirmed in a longer time-course in (**b**), shown as mean +/- SEM, n =3 and analyzed by Two-Way ANOVA, time p<0.001, *Ck1δ1* vs *Ck1δ2* p<0.01, interaction p<0.001. Bonferroni post-hoc significances were: ***=p<0.0001, **=p<0.01, *=p<0.05. Real data points are shown on the graph, but one-phase decay non-linear fit estimated the half-life of *Ck1δ1* and *Ck1δ2* to be 1.4h and 3.6h, respectively. (**c**) The 3'-UTR of *Ck1δ* transcripts is a negative regulator of translation. On top, electrophoresis of in vitro-transcribed mRNAs to confirm specificity of transcription before in vitro translation in reticulocyte lysates and luminescence quantification at the bottom, with transcript structure indicated. Data analyzed by One-way ANOVA followed by Bonferroni post-test, shown mean +/- SEM, n=4, a vs. b p<0.001, a vs. c, p<0.01, c vs. b p<0.001.

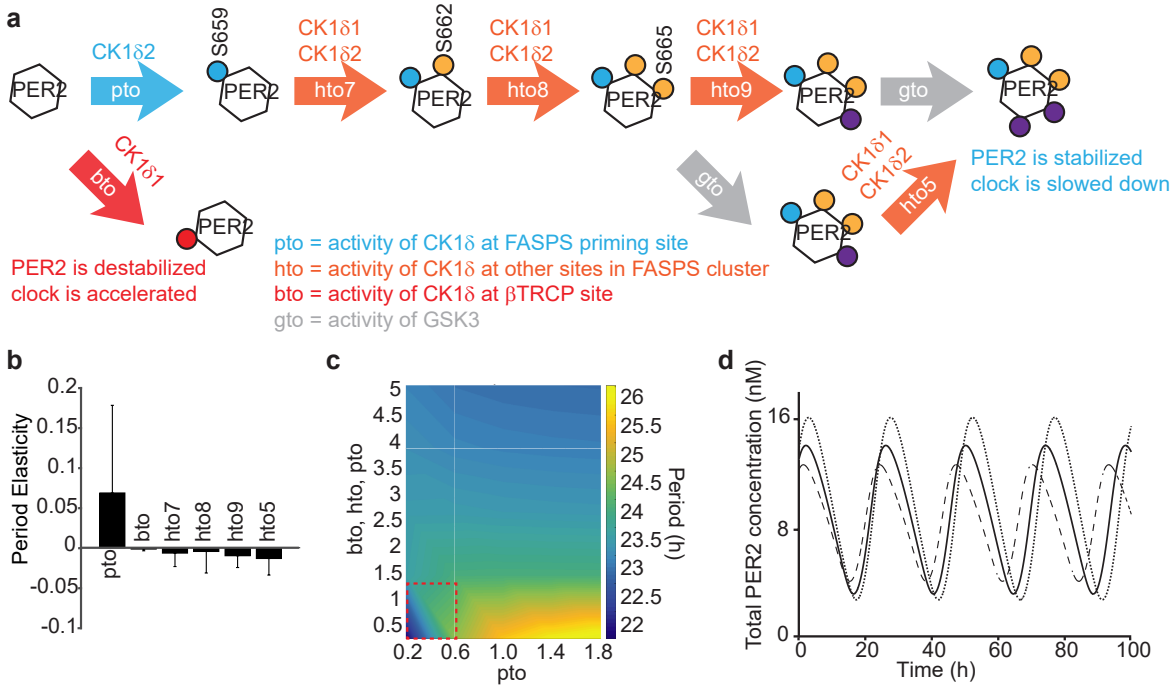

Fig. S3: Mathematical modelling predicts CK1δ2 is the priming kinase

(**a**) Base model of branched PER2 phosphorylation paths, with the bto branch (CK1 phosphorylation rate constant at β-TrCP site) and the pto branch (priming kinase phosphorylation rate constant) leading to opposite regulation of PER2 fate, and therefore circadian period. The hto steps, dependent on priming at S659, are CKI-mediated phosphorylation rate constants. The gto steps, included in the original model, are mediated by another kinase (GSK3) and will not be discussed here. Based on our model and data, proposed CK1δ isoforms mediating each phosphorylation step is indicated on top of each arrow. (**b**) Circadian period became longer (i.e. positive elasticity) only when pto was increased, but independently increasing subsequent steps in the same branch (hto) lead to short period, like bto. Period (τ) elasticity is plotted with its standard deviation for 100 computations. (**c**) Calculated circadian period became shorter when the pto rate was decreased, but if bto, hto and pto decrease in concert (Ck1δ knock-out for example), period elongates. (d) Predicted wave-forms when pto rate is changed: broken line, rate=0.192; solid, 0.383 (original); dotted, 1.53.

a

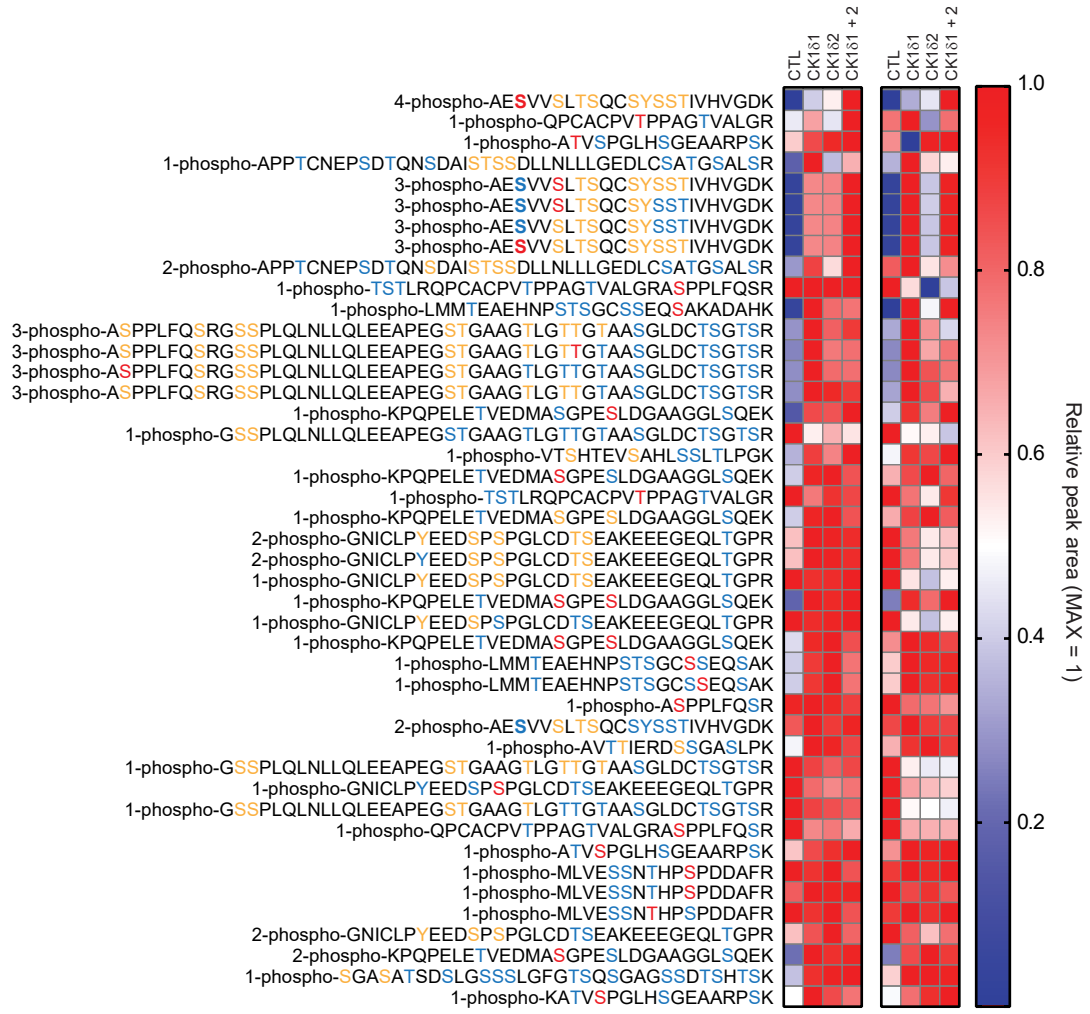

b

(1) 3-phospho-AESVVpS[662]LTSQCSYSSTIVHVGDK

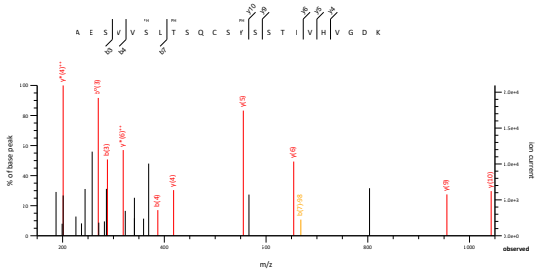

(4) 3-phospho-AEpS[659]VVSLTSQCSYSSTIVHVGDK

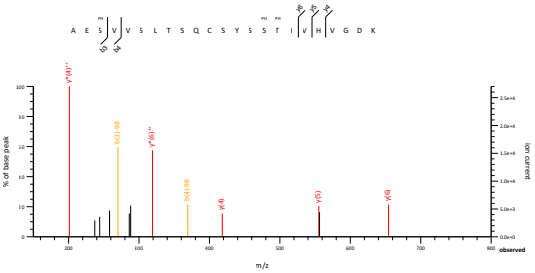

(2) 3-phospho-AESVVSLTSQCSYSSTIVHVGDK

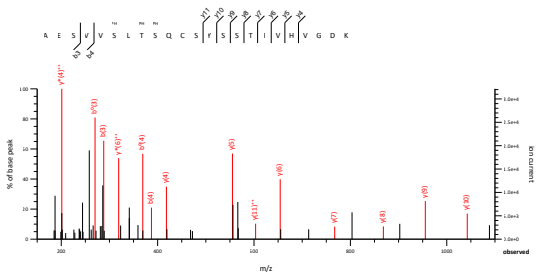

(5) 2-phospho-AESVVSLTSQCSYSSTIVHVGDK

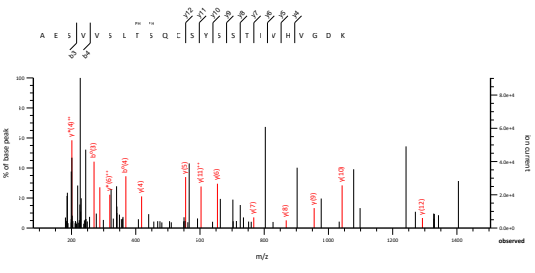

(3) 3-phospho-AESVVSLTSQCSYSSTIVHVGDK

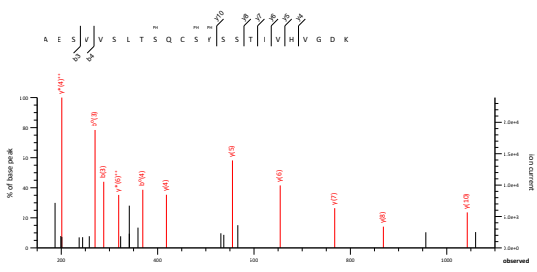

(6) 4-phospho-AEpS[659]VVSLTSQCSYSSTIVHVGDK

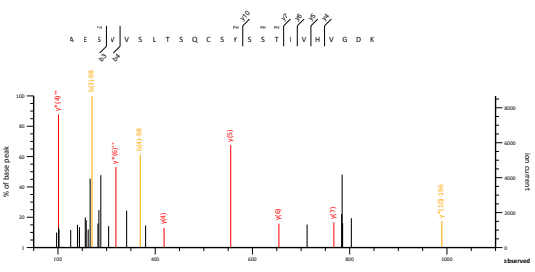

Fig. S4: CK1δ1 and CK1δ2 cooperate in phosphorylating PER2.

(**a**) Semi-quantitative results displayed as a heat map of CK1δ isoforms-dependent PER2 phosphopeptides abundance. Here, all phosphorylated PER2 peptides detected are shown, sorted from top to bottom in order of their mean fold changes in the three columns with CK1δ vectors. Data from two technical replicates are provided, side-by-side. The column labels indicate the vectors co-transfected with 5xMYC-PER2. The total amount of phosphate moieties is indicated as a prefix in the row labels, showing the phosphopeptide sequence. Note the tetraphosphorylated FASPS peptides at the top. Confirmed phosphosites and non-phosphosites were labeled in red and blue, respectively. Ambiguous phosphosites were labeled in yellow. (**b**) MS/MS spectra of AESVVSLTSQCSYSSTIVHVGDK (FASPS) peptides. (1) to (4) show the spectra of four alternative 3-phosphopeptides shown in Fig. S4a; (5), 2-phosphopeptide; (6), 4-phosphopeptide.

References

1. Etchegaray JP, et al (2009) Casein kinase 1 delta regulates the pace of the mammalian circadian clock. *Mol Cell Biol* 29(14): 3853-3866.
2. Lee JW, et al (2011) A small molecule modulates circadian rhythms through phosphorylation of the period protein. *Angew Chem Int Ed Engl* 50(45): 10608-10611.
3. Zhou M, Kim JK, Eng GW, Forger DB & Virshup DM (2015) A Period2 phosphoswitch regulates and temperature compensates circadian period. *Mol Cell* 60(1): 77-88.
4. Daub H, et al (2008) Kinase-selective enrichment enables quantitative phosphoproteomics of the kinome across the cell cycle. Mol Cell 31(3): 438-448.
5. Oppermann FS, et al (2009) Large-scale proteomics analysis of the human kinome. *Mol Cell Proteomics* 8(7): 1751-1764.
6. Lee C, Weaver DR & Reppert SM (2004) Direct association between mouse PERIOD and CKIepsilon is critical for a functioning circadian clock. *Mol Cell Biol* 24(2): 584-594.
7. Kannan N, Haste N, Taylor SS & Neuwald AF (2007) The hallmark of AGC kinase functional divergence is its C-terminal tail, a cis-acting regulatory module. *Proc Natl Acad Sci* U S A 104(4): 1272-1277.
8. Penas C, et al (2014) Casein kinase 1delta-dependent Wee1 protein degradation. *J Biol Chem* 289(27): 18893-18903.
9. Graves PR & Roach PJ (1995) Role of COOH-terminal phosphorylation in the regulation of casein kinase I delta. *J Biol Chem* 270(37): 21689-21694.
10. Zhao B, Nachtergaele S, Roundtree IA & He C (2018) Our views of dynamic N(6)-methyladenosine RNA methylation. *RNA* 24(3): 268-272.
11. Darnell RB, Ke S & Darnell JE,Jr (2018) Pre-mRNA processing includes N6 methylation of adenosine residues that are retained in mRNA exons and the fallacy of "RNA epigenetics". *RNA* 24(3): 262-267.
12. Yoo SH, et al (2004) PERIOD2::LUCIFERASE real-time reporting of circadian dynamics reveals persistent circadian oscillations in mouse peripheral tissues. *Proc Natl Acad Sci* U S A 101(15): 5339-5346.
13. Huang Y, McNeil GP & Jackson FR (2014) Translational regulation of the DOUBLETIME/CKIdelta/epsilon kinase by LARK contributes to circadian period modulation. *PLoS Genet* 10(9): e1004536.
14. Eide EJ, et al (2005) Control of mammalian circadian rhythm by CKIepsilon-regulated proteasome-mediated PER2 degradation. *Mol Cell Biol* 25(7): 2795-2807.
15. Tainaka M, Doi M, Inoue Y, Murai I & Okamura H (2018) Circadian PER2 protein oscillations do not persist in cycloheximide-treated mouse embryonic fibroblasts in culture. *Chronobiol Int* 35(1): 132-136.
16. Fustin JM, et al (2013) RNA-methylation-dependent RNA processing controls the speed of the circadian clock. *Cell* 155(4): 793-806.
17. Trapnell C, et al (2012) Differential gene and transcript expression analysis of RNA-seq experiments with TopHat and cufflinks. *Nat Protoc* 7(3): 562-578.

18. Zhang Y, et al (2008) Model-based analysis of ChIP-seq (MACS). *Genome Biol* 9(9): R137-2008-9-9-r137. Epub 2008 Sep 17.
19. Heringa J (1999) Two strategies for sequence comparison: Profile-preprocessed and secondary structure-induced multiple alignment. *Comput Chem* 23(3-4): 341-364.
20. Cong L, et al (2013) Multiplex genome engineering using CRISPR/cas systems. *Science* 339(6121): 819-823.
21. Ruoff P (1992) Introducing temperature-compensation in any reaction kinetic oscillator model. *Journal of Interdisciplinary Cycle Research* 23(2): 92-99.
22. Rappsilber J, Mann M & Ishihama Y (2007) Protocol for micro-purification, enrichment, pre-fractionation and storage of peptides for proteomics using StageTips. *Nat Protoc* 2(8): 1896-1906.